Development of A Family of High Voltage Gain Step-Up Multi-Port DC-DC Converters for Fuel Cell-based Hybrid Vehicular Power Systems

Pouya Zolfi, Sina Vahid, Ayman EL-Refaie
Werner's Sustainable Energy Lab - MARQUETTE UNIVERSITY
Engineering Hall (EH261), 1250 W Wisconsin Ave, 53233
Milwaukee, WI, USA
Tel.: +1 (414) 288-1940
E-Mail: pouya.zolfi@marquette.edu

Keywords

«DC-DC power converter», «Electric vehicle», «Energy storage», «Fuel Cell», «Power management»

Abstract

Battery assisted fuel cell based vehicular power systems are feasible solutions for transportation electrification. Step up DC-DC converters play an important role in energy conversion process of these systems. Due to uncertain nature and low voltage level of fuel cells, large voltage gain converters are desired. This paper proposes a family of non-isolated step-up DC-DC multi-port converters for hybrid FC + battery vehicular power systems with smart grid services capability. Fewer active and passive components compared to other step-up topologies in the literature, extendibility, simple power flow management, and low current and voltage ripples are among the benefits of this multi-port converter family. Design and control of these converters are discussed, and the simulations are conducted for one of the proposed topologies. In the simulation scenario, a 60-kW FC + battery vehicle system is used as the baseline for real-world application. The simulation results demonstrate the effectiveness of this step-up multi-port converter and the peak efficiency of 95.6% was recorded. Also, a lab-scale prototype of the converter is built and tested under various power flow scenarios to validate the simulation results.

Introduction

Step-up DC-DC converters play an important role in energy conversion process of renewable energy systems (RESs) and energy storage systems (ESSs). Due to low voltage levels of the mentioned systems, high voltage gain converters are required to reach system level voltages. Furthermore, low-ripple input current should be provided to increase power quality on both generation and consumption sides. High step-up DC-DC topologies are divided into two main categories: isolated and non-isolated. The main demerit of isolated high step-up converters is their transformers' high weight and volume [1]. Non-isolated high step-up converters are mostly based on coupled inductor technologies. By adjusting turn ratio of the coupled inductor and implementation of switched capacitor technique, these converters can achieve high voltage gains [2]. Effects of the leakage inductance on power switches' stress, reverse recovery problem of diodes, and high volume and cost of the converter are regarded as the main drawbacks of the coupled inductor-based high gain step-up topologies [3]. In [4], a quadratic coupled inductor-based high gain step-up DC-DC converter is proposed for RESs applications. High number of circuit components is the main demerits of this circuit. In [4], an extendable non-isolated ultra-high step-up topology is discussed for renewable energy applications. High number of components in [5] has led to a bulk and complex structure. Other non-isolated topologies are presented in [6-8], which suffer from one or more of the mentioned issues. The other type of the non-isolated high step-up DC-DC converters is based on cascading basic topologies and switched capacitor/switched inductor techniques. Large gain step-up non-isolated converters based on geometric structures are discussed in [9].
Benefiting from fewer active and passive components, multi-port converters (MPCs) are considered an effective solution for the integration of RESs and ESSs and can similarly be categorized into isolated and non-isolated types. In [10, 11], two new isolated topologies for three-port DC-DC converters (TPCs) are proposed for DC microgrid application but has high number of power switches. A new MPC based

on push-pull converter is introduced in [12] for the auxiliary power unit of refrigerated vehicles with assistance of three inductors (cores) and four power switches which leads to a bulk topology in high power levels. A non-isolated coupled inductor-based TPC is presented in [13] for fuel-cell electric vehicle (FCEV) applications. Apart from the coupled inductor-initiated problems, this converter is not flexible and/or extendable and the energy management scheme is not discussed. Another non-isolated MPC is proposed by authors in [14] for hybrid streetcar application. The comprehensive energy management scheme is introduced, but the converter suffers from high current ripple in at least one of the input ports. In order to develop MPCs, this study uses systematic design approaches presented in [15, 16] which is suitable for a wide range of applications.

This paper presents a family of low switch count non-isolated continuous input current step-up DC-DC converters for single-input single-output (SISO) and multi-input multi-output (MIMO) systems. Although the major focus of this paper is on FC-based e-mobility, the proposed MPC is capable of being used in a wide range of applications. A battery-assisted hybrid vehicular FC power system is considered, with mileage extension and smart grid services. The baseline and MPC-based FC + battery systems are shown in Fig. 1(a) and (b), respectively. Proposed topologies provide high voltage gains with proper duty cycle values in addition to low ripple input current/output voltage and high efficiency values. Simulation results using PLECS® software are validated with the lab-scale converter prototype.

The rest of the paper is organized as follows: The development process of the proposed converters is discussed in the upcoming section. Integration scenarios and energy management scheme are discussed next. Simulation and experimental verifications and finally the conclusions are presented.

Development and Analysis of The Converter Topologies

Fundamental Step-up Converter Topology (Single Input Single Output - SISO)

The fundamental high gain step-up converter is a single switch topology that consists of two inductors, four capacitors and five diodes as shown in Fig.2. L_1 is the input side inductor and guarantees the continuity of input current that is regarded as an important factor for renewable energy integration. This topology is derived using boost and voltage multiplier building blocks (BBs) and presents a wide range voltage conversion ratio with proper switching duty cycle values. C_4 is considered as the output side capacitor and provides nearly-zero ripple voltage for load terminals. Output side diode D_5 also prevents

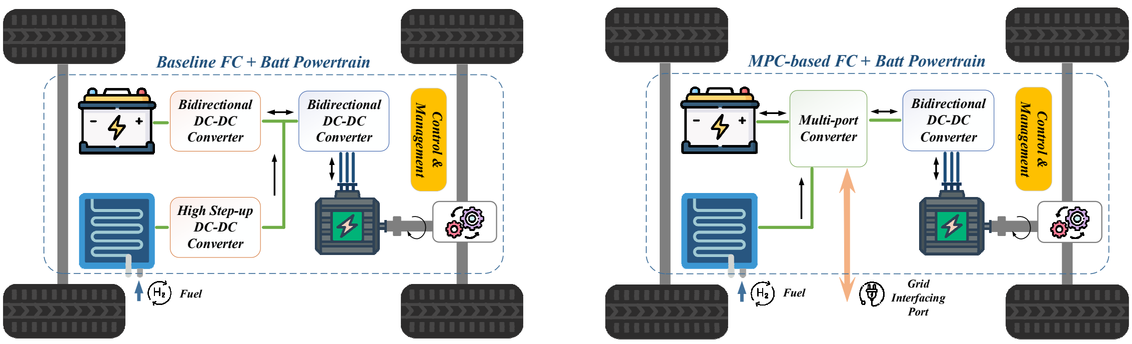

(a) (b)

Fig. 1: A battery-assisted hybrid vehicular FC power system (a) baseline design and (b) MPC-based

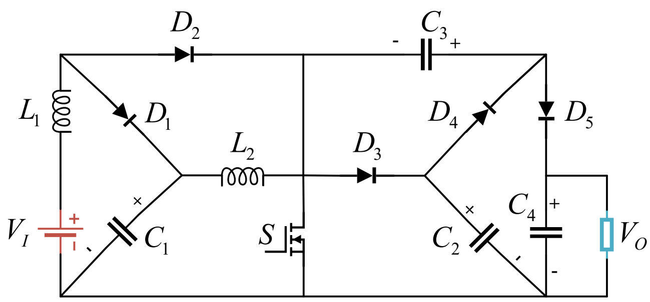

Fig. 2: Baseline fundamental SISO topology

unwanted power flow from load side to the input side in the case of active load. To simplify the analysis, following assumptions are considered:

- Capacitors C_1, C_2, C_3, and C_4 are large and their voltages are considered to be constant during one switching period, and
- ESR resistances of capacitors and inductors are neglected in steady state analysis but are considered for efficiency studies.

The operating modes of the high step-up SISO converter and the related waveforms during continuous conduction mode (CCM) are shown in Fig. 3. The converter has two operating modes in CCM which are discussed as follows:

Mode 1 [$0 \le t < DT_S$ **]** This mode starts by turning on the power MOSFET. L_1 is charged by V_I through D_2 and S. C_1 that has been charged from previous switching period is discharged to L_2 through S. Furthermore, C_2 is discharged through D_4 to charge C_3. D_1, D_3, and D_5 are reverse biased in this mode and output capacitor (C_4) feeds the load. This mode ends when the power MOSFET is turned off. Following equations are derived for this operation mode:

$$V_{L1} = V_I \tag{1}$$

$$V_{L2} = V_{C1} \tag{2}$$

$$V_{C2} = V_{C3} \tag{3}$$

Mode 2 [$DT_S \le t < T_S$ **]** In this mode, the power MOSFET is off and D_1 and D_3 are forward biased. C_1 is charged by V_I and L_1 through D_1. L_2 charges C_2 through D_3. D_5 is conducting in this mode and provides a path from C_3 to output for charging C_4 and feed the load side. This mode continues until power MOSFET is switched on. Equations related to this mode are presented as follows:

$$V_{L1} = V_I - V_{C1} \tag{4}$$

$$V_{L2} = V_{C1} - V_{C2} \tag{5}$$

$$V_{C2} = V_O - V_{C3} \tag{6}$$

By applying volt-seconds balance principle on the inductors, following equations are derived which leads to the CCM voltage gain equation of the SISO topology.

$$DV_I + (1-D)(V_I - V_{C1}) = 0 \;\rightarrow\; V_{C1} = \frac{V_I}{1-D} \tag{7}$$

$$DV_{C1} + (1-D)(V_{C1} - V_{C2}) = 0 \;\rightarrow\; V_{C2} = \frac{V_{C1}}{1-D} = \frac{V_I}{(1-D)^2} \tag{8}$$

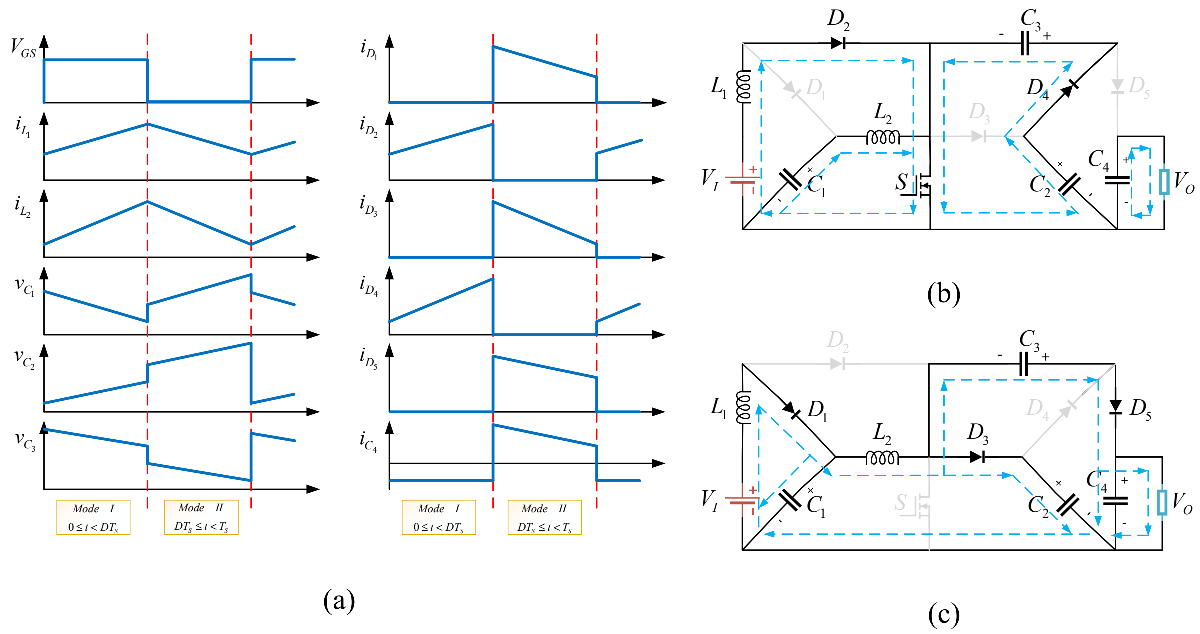

(a) (b) (c)

Fig. 3: (a) CCM waveforms, (b) mode I and (c) mode II for the SISO topology during CCM

$$\begin{cases} V_{C3} = V_{C2} \\ V_O = V_{C2} + V_{C3} \end{cases} \rightarrow M_{CCM} = \frac{V_O}{V_I} = \frac{2}{(1-D)^2} \tag{9}$$

Similar analysis can be provided for discontinuous conduction mode (DCM) operation of the SISO converter. The converter has one additional operating mode during DCM which is when all semiconductor switching components are off, i.e. all diodes are reverse biased in this mode and power MOSFET is also in off state. Load is fed only by output capacitor C_4, that has been charged from previous operating mode. This mode ends when the power MOSFET is turned on in the next switching period. $D^{'}$ is considered as the time interval that inductors' currents decrease from their maximum value to zero. By applying volt-seconds balance principle on the inductors, following equations are derived:

$$DV_I + D^{'}(V_I - V_{C1}) = 0 \;\rightarrow\; V_{C1} = (1 + \frac{D}{D^{'}})V_I \tag{10}$$

$$DV_{C1} + D^{'}(V_{C1} - V_{C2}) = 0 \;\rightarrow\; V_{C2} = (1 + \frac{D}{D^{'}})^2 V_I \tag{11}$$

$$\begin{cases} V_{C3} = V_{C2} \\ V_O = V_{C2} + V_{C3} \end{cases} \rightarrow M_{DCM} = \frac{V_O}{V_I} = 2(1 + \frac{D}{D^{'}})^2 \tag{12}$$

Average currents of the capacitors in one switching period are zero. Also, average current of the diode D_5 is equal to the average output (load) current, hence:

$$I_O = \frac{1}{2} D^{'} I_{D5} \tag{13}$$

$$I_O = \frac{V_O}{R_L} \tag{14}$$

$$I_{D5} = \frac{V_I}{L_T f_S} \tag{15}$$

$$L_T = L_1 + L_2 \tag{16}$$

By replacing (14) in (13) and then (13) in (15), respectively, following equations are obtained:

$$D^{'} = M_{DCM} \frac{2L_T f_S}{DR_L} \tag{17}$$

$$\tau = \frac{L_T f_S}{R_L} \tag{18}$$

Where τ is the normalized time constant of the inductor. By replacing (17) in (12), simplification and using (18), a new form of voltage gain relation during DCM is derived as follows:

$$M_{DCM} = \sqrt{1 + 4\frac{D^2}{\tau}} \tag{19}$$

Boundary conduction mode (BCM) is the common mode between CCM and DCM. Therefore, by equalizing (9) and (19), boundary normalized time constant of the inductor, τ_B is obtained as follows.

$$M_{CCM} = M_{DCM} \Rightarrow \tau_B = \frac{(1-D)^4 .4D^2}{4 - (1-D)^4} \tag{20}$$

τ_B curve in terms of duty cycle is presented in Fig.4 for the conventional boost converter, converter presented in [3] (as an example of modern single-switch high step-up converters) and the baseline SISO converter to evaluate the ability of converters for operation in CCM. Suggested converter would operate in CCM – that is favorable – for $\tau > \tau_B$. This figure shows that the high step-up SISO converter operates in CCM for a broader range of duty cycle values in comparison with other topologies.

The values of inductors and capacitors are calculated based on steady-state analysis to guarantee CCM operation and ripple requirements of the SISO topology. Using (18) and (20), following equation for equivalent inductance is derived. During the design process, L_2 is obtained based on the load requirements, as presented in (22). Then L_1 can be calculated based on (16).

$$L_T \geq \frac{R_L}{f_S}\frac{4D^2(1-D)^4}{4-(1-D)^4} \tag{21}$$

$$L_2 \geq \frac{R_L}{f_S}\frac{D(1-D)^2}{4} \tag{22}$$

Output side capacitor value for CCM operation is obtained by following equations:

$$V_{C_4}(DT_S) = V_{C_4}(0) + \frac{1}{C_4}\int_0^{DT_S} i_{C_4}(t).dt \Rightarrow \Delta V_{C_4} = \frac{DV_O}{C_4 R_L f_S} \Rightarrow C_4 \geq \frac{DV_O}{\Delta V_{C_4} R_L f_S} \tag{23}$$

Similarly, by deriving current equations for the capacitors C_1, C_2, and C_3 the capacitor values can be calculated as shown in (24) and (25).

$$C_1 \geq \frac{2DV_O}{\Delta V_{C_1}(1-D)(1-2D)R_L f_S} \tag{24}$$

$$C_{2\&3} \geq \frac{V_O}{\Delta V_{C_{2\&3}}(1-2D)R_L f_S} \tag{25}$$

Discussed SISO topology provides higher voltage gain for a specific duty cycle value in comparison to similar high step-up topologies. Table I shows a thorough comparison between suggested converter and similar converters which are introduced in literature. Fig.5 provides gain curves for the mentioned topologies. This figure shows that for $D \geq 0.5$, voltage gain of the discussed topology is more outstanding in comparison with other structures.

Step-up Multi-port Converter Topologies (Multiple Input Multiple Output – MIMO)

A family of step-up MPCs can be developed based on the SISO topology. Fig. 6(a) illustrates a unidirectional MIMO topology with only one power switch. This topology is capable of utilizing two input ports and two output ports to integrate RESs. Power flow is unidirectional in the abovementioned converter which makes it more suitable for low- to medium-power renewable energy systems. By replacing one of the power diodes with the combination of diode-power MOSFET, bidirectional power flow can be achieved. Fig. 6(b) shows the bidirectional MIMO MPC, which can be used in ESS applications and is the main topology considered in this study for the battery-assisted hybrid vehicular FC power system. As discussed before, the proposed converter is developed based on the fundamental DC-DC BBs, thus, this family of step-up MPCs is capable of being extended by adding/replacing the BBs. The possible operating modes and related voltage gain relationships for the proposed bidirectional

Table I: Comparison between the SISO topology and other similar converters

Converter / Parameter	Boost	SISO Converter	[3]	[17]	[18]	[19]	[20]
CCM Gain	$\frac{1}{1-D}$	$\frac{2}{(1-D)^2}$	$\frac{3+D}{2(1-D)}$	$\frac{2+n}{1-D}; n=2$	$\frac{3+D}{1-D}$	$\frac{1+D}{1-D}$	$\frac{n}{D(1-D)}; n=2$
# Inductor core	1	2	2	2	2	2	2
# Diode	1	5	4	3	5	4	4
# Switch	1	1	1	1	1	1	2
# Capacitor	1	4	4	4	4	1	4
Maximum Input Current Ripple %	25	20	22.5	20	200	75	20
Peak η %	93.4	95.6	93.1	97	95	83	97

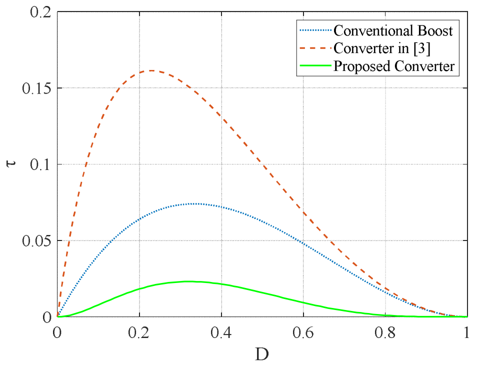

Fig. 4: Curve for the normalized time constant of inductor in terms of duty cycle values

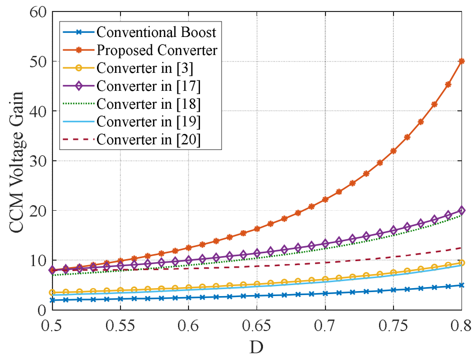

Fig. 5: Voltage gain comparison graphs

MIMO topology are presented in Fig.7 and Table II, respectively.

Integration Scenarios and Energy Management Scheme

A variety of source-load integration modes are possible by implementing the proposed MIMO topology. Seven modes of integration are defined for the MIMO topology in a hybrid FC + battery vehicular power

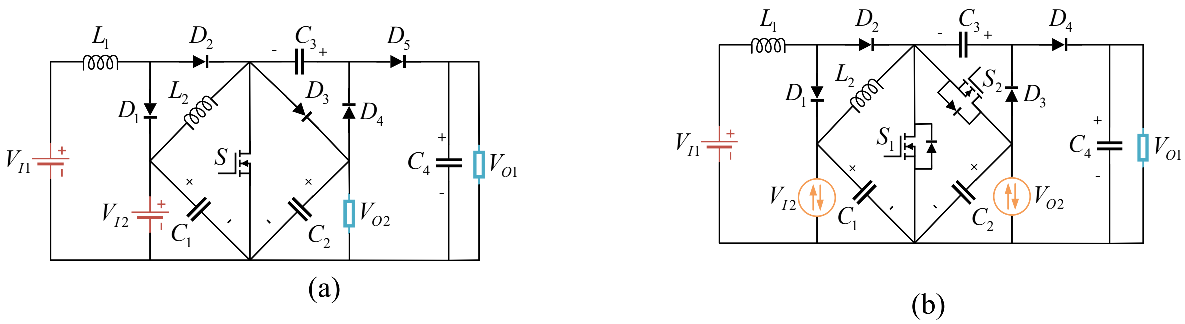

Fig. 6: MIMO topologies (a) unidirectional, and (b) bidirectional

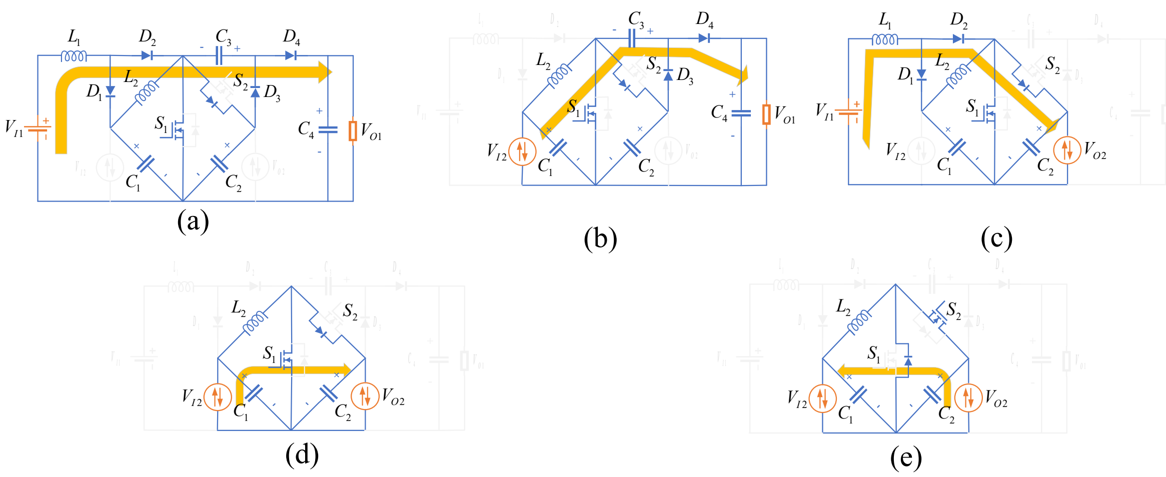

Fig. 7: Operating modes for the bidirectional MIMO topology

Table II: Voltage gain equations for the bidirectional MIMO topology

Mode	M_a	M_b	M_c	M_d	M_e
Voltage Gain	$\frac{V_{O_1}}{V_{I_1}} = \frac{2}{(1-D)^2}$	$\frac{V_{O_1}}{V_{I_2}} = \frac{2}{1-D}$	$\frac{V_{O_2}}{V_{I_1}} = \frac{1}{(1-D)^2}$	$\frac{V_{O_2}}{V_{I_2}} = \frac{1}{1-D}$	$\frac{V_{I_2}}{V_{O_2}} = D$

system. Fig. 8(a) presents the system configuration implementing the bidirectional MIMO converter and Fig. 8(b) summarizes the possible modes among the main ports and the reconfigurable converter types.

Scenario 1 [FC to Motor]: This is the main operating scenario and occurs when the FC tank is full. As shown in Fig. 7(a), switch S_1 is the only active power switch during this mode and the proposed MIMO acts as a high step-up converter with full voltage gain utilization.

Scenario 2 [FC to Battery]: In the no load condition, when the FC has the capability of providing excessive power and the battery is fully depleted, this scenario occurs. The battery is charged by C_1 through L_1 and D_1.

Scenario 3 [FC to Grid]: This mode has the lowest priority and occurs only in the no load condition where the battery is fully charged, and grid demands power, i.e. vehicle to grid (V2G) services. This scenario is shown in Fig. 7(c). The electronic contactor is in position A during this mode.

Scenario 4 [Battery to Motor]: When the FC is not available, the backup battery provides power to the load side. As shown in Fig. 7(b), S_1 is the active switch during this mode. It has to be mentioned that the backup battery can feed the load for a limited period of time due to the small capacity.

Scenario 5 [Motor to Battery]: Bidirectional port of the MIMO converter (V_{O2}) is utilized to charge the back-up battery pack during regenerative braking (electronic contactor in position B). This mode is shown in Fig. 7(e), where S_2 is the active switch and converter behaves as a step-down topology.

Scenario 6 [Grid to Battery]: The proposed bidirectional MIMO topology is capable of providing grid to vehicle (G2V) services. The backup battery can be charged by the grid interface connection. This mode is similar to the previous scenario, except here the electronic contactor in position A.

Scenario 7 [Battery to Grid]: This scenario also addresses the G2V service providing capability of the proposed converter. This mode is shown in Fig. 7(d), where the battery is connected to the grid interface through a boost building block via the electronic contactor in position A.

Energy management scheme for the MIMO converter-based FC + battery vehicular power system is presented in Fig. 9. At the first stage, the motor status is checked to determine its operating mode. Next stage determines the availability of the FC stacks. If available, FC is the main power source and is preferred over the other resources. In the third stage, state of charge (SOC) of the battery is obtained by

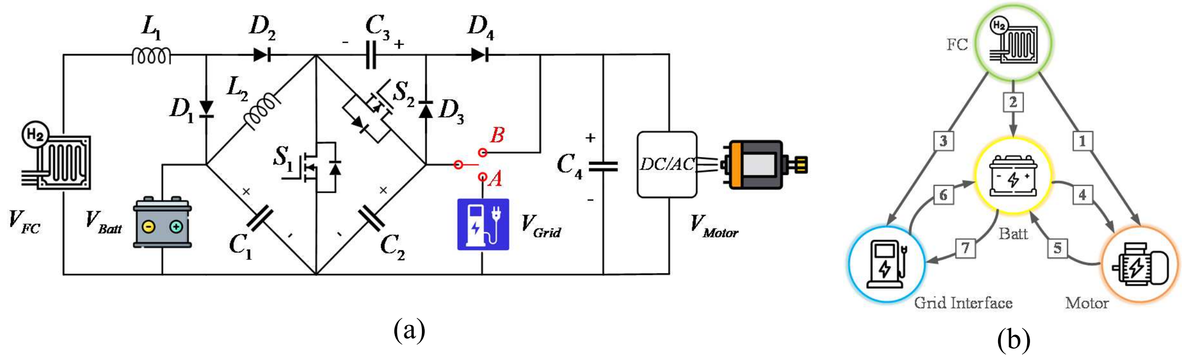

Fig. 8: (a) Proposed converter for FC-based vehicular powertrain (b) Integration scenarios

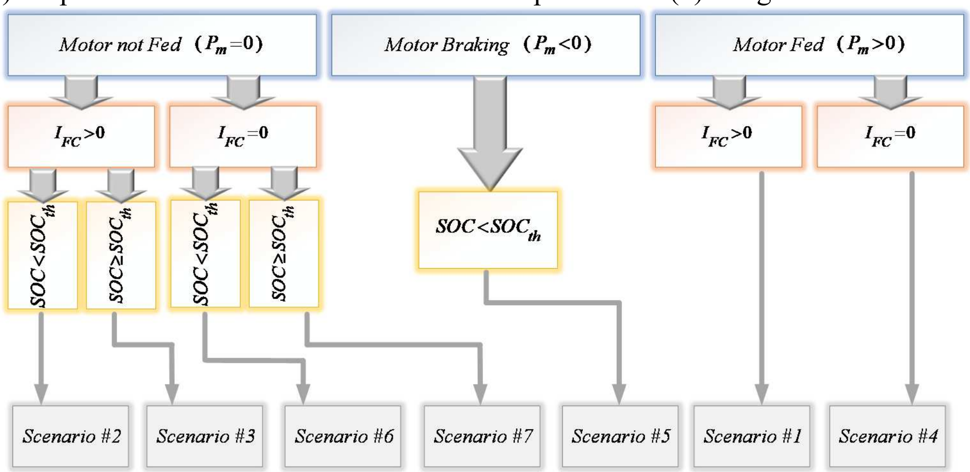

Fig. 9: Decision chart for the proposed MIMO-based power system

its current and voltage, and then the SOC is given to the control unit to make the final decision and determine the scenario of operation. The battery is the emergency power provider. Charging and discharging processes are defined and the suitable control decision can be made by a comparison between the battery's SOC and the threshold SOC (SOC_{th}).

Simulation and Experimental Validation

Simulation of the proposed converter using PLECS® software demonstrates the effectiveness of the theoretical analysis. Simulations are conducted for a 60-kW system which is typical for a medium size FCEV. The switching frequency is 50kHz in this simulation. The FC stacks and motor side DC link voltages are considered to be 100 V and 800 V, respectively. A 200 V – 60 kWh battery pack is modeled for the FCEV system. Grid interface port voltage is 400 V which is selected based on the voltage level standards in DC distribution networks [21]. Fig. 10(a) and 10(b) present the voltage and current waveforms for the FC and motor side DC link, respectively, with 50% duty cycle. Proposed converter is capable of providing nearly-zero input/output current/voltage ripples which increases FC stack lifetime [22] and simplifies the motor speed control procedure. High frequency current ripple leads to sharp increase in the high-frequency resistance (HFR) which is identified as a severe degrading condition for FC stacks. A maximum efficiency of 95.6% is recorded for the simulations (scenario 7 shown in Fig. 7(d)) considering the thermal models of semiconductors and ESR resistances of the passive components. Loss distribution among various components during this mode is shown in Fig. 11.

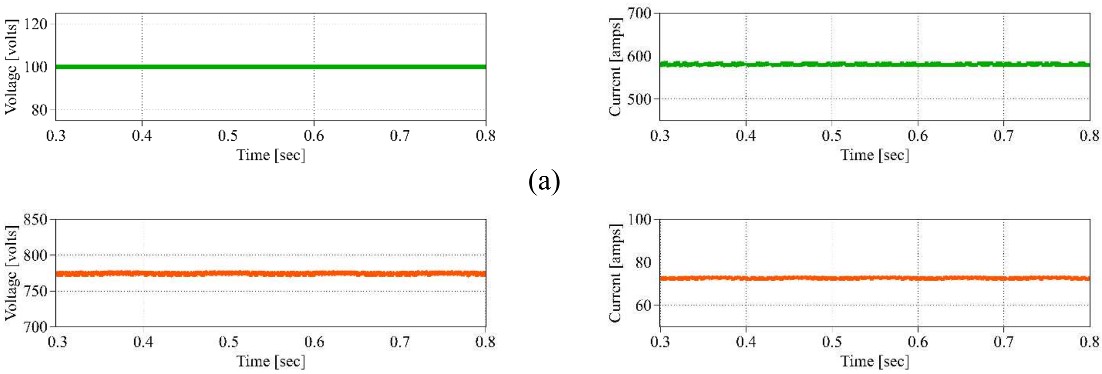

Fig. 10: Simulation results for (a) FC and (b) Motor side

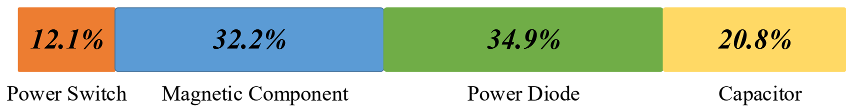

Fig. 11: Loss distribution diagram for the peak efficiency case (scenario 7)

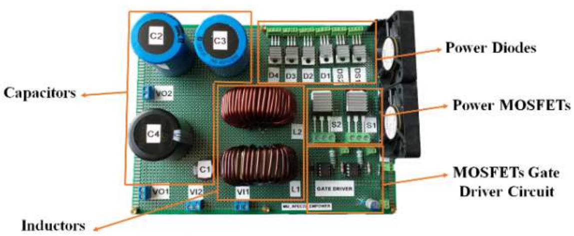

Fig. 12: 1-kW prototype of the bidirectional MIMO

Table II: Prototype Specifications

Spec/ Component	Value/ Type
V_{I1}, V_{I2}	30 V, 60 V
V_{O1}, V_{O2}	240 V, 120 V
L_1, L_2	174 µH, 311 µH
C_1	200 V – 100 µF
C_2, C_3	400 V – 680 µF
C_4	600 V – 220 µF
D_1, D_2	V30202C-M3/4W
D_{S1}, D_{S2}, D_3	SBR40U300CT
D_4	SBR40U300CT-G
S_1	IXFH120N30X3
S_2	IXFQ72N30X3

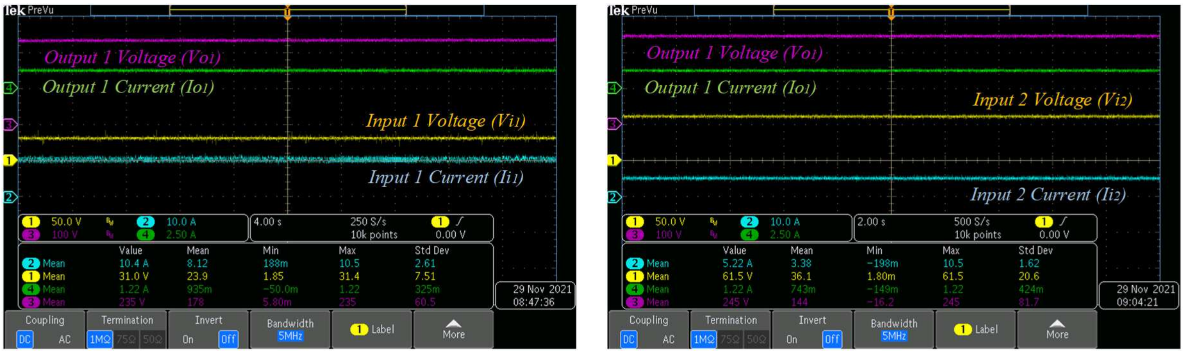

(a) (b)

Fig. 13: Experimental results for scenarios 1 and 4

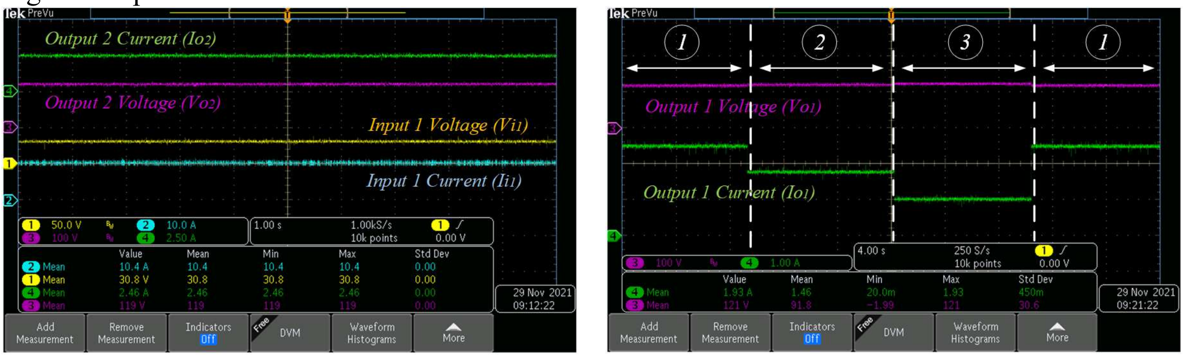

(a) (b)

Fig. 14: Experimental results for scenario 3 (a) waveforms and (b) transient behavior

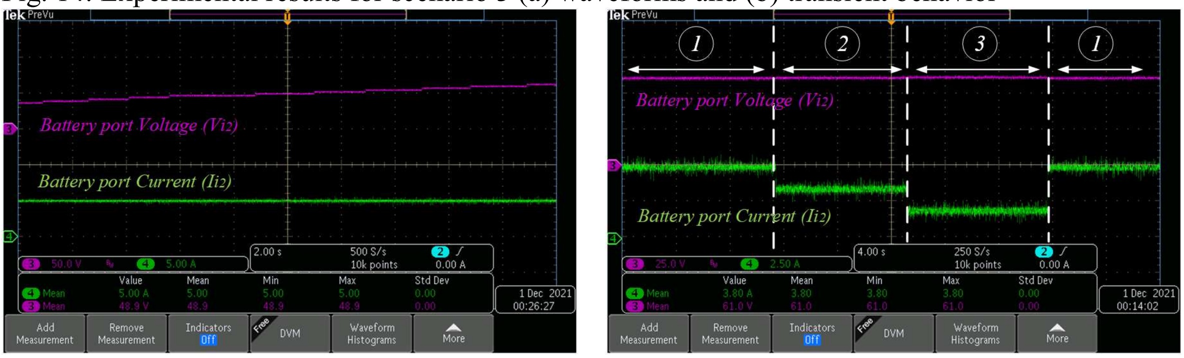

(a) (b)

Fig. 15: Experimental results for battery charging (a) CC and (b) CV scenarios

A lab-scale prototype of the proposed converter is built and tested for various integration scenarios and is shown in Fig. 12. The implemented converter is tested for 300 W power level (Peak efficiency of 96.7%). Table III provides the detailed specification of the developed converter prototype. Fig.13(a) and 13(b) present the experimental results for scenarios no.1 (FC to motor; based on the diagram presented in Fig. 8(b)) and no.4 (battery to motor), respectively. For FC to grid-side scenario, experimental voltage and current waveforms are recorded and presented in Fig.14(a), while the transient behavior of the proposed MPC for a variable current case is presented in Fig.14(b). The converter is capable of supplying the load with a constant low-ripple voltage which improves the power quality of the grid interaction. Fig.15(a) shows the results for a constant current (CC) battery charging scenario (integration scenario no.6), where the battery voltage increases gradually as its SOC increases. On the other hand, the constant voltage (CV) case scenario is also tested and is shown in Fig.15(b).

Conclusion

In this paper, a family of high voltage gain step-up DC-DC MPCs is introduced, briefly analyzed, simulated and tested. SISO, unidirectional MIMO, and bidirectional MIMO extensions are discussed. Proposed topologies have lower number of power switches in comparison to the similar structures in the literature. Furthermore, high simulation efficiency (95.6% peak value), high voltage gain, nearly-zero voltage and current ripple in both input and output ports, extendable architecture for a wide range of applications, and a simple management scheme are regarded as the main advantages of the proposed converters. Bidirectional MIMO topology was considered as the main interface in a battery-assisted FCEV powertrain application and respective simulations performed for a 60-kW system which indicate the effectiveness of the proposed converter. A lab scale 300 W prototype is implemented to verify the operation of the proposed power converter. Peak efficiency of 96.7% is recorded for this low-power prototype. Several integration scenarios are tested, and results are compatible with the simulation and analytical analysis.

References

[1] S. S. Sayed and A. M. Massoud, "Review on State-of-the-Art Unidirectional Non-Isolated Power Factor Correction Converters for Short-/Long-Distance Electric Vehicles," in IEEE Access, vol. 10, pp. 11308-11340, 2022, doi: 10.1109/ACCESS.2022.3146410.

[2] F. Barmoudeh, P. Zolfi, S. Karami and A. Ajami, "A Novel High Power High Step up DC-DC Converter with Parallel Structure", *order*, vol. 2, pp. D3.

[3] S. Saravanan and N. R. Babu, "Design and Development of Single Switch High Step-Up DC–DC Converter," in IEEE Journal of Emerging and Selected Topics in Power Electronics, vol. 6, no. 2, pp. 855-863, June 2018, doi: 10.1109/JESTPE.2017.2739819.

[4] S. A. Modaberi, B. Allahverdinejad and M. R. Banaei, "A Quadratic High Step-up DC-DC Boost Converter Based on Coupled inductor with Single Switch and Continuous Input Current," 2021 12th Power Electronics, Drive Systems, and Technologies Conference (PEDSTC), 2021, pp. 1-6, doi: 10.1109/PEDSTC52094.2021.9405958.

[5] P. Mohseni, S. Rahimpour, M. Dezhbord, M. R. Islam and K. M. Muttaqi, "An Optimal Structure for High Step-Up Non-Isolated DC-DC Converters with Soft-Switching Capability and Zero Input Current Ripple," in IEEE Transactions on Industrial Electronics, doi: 10.1109/TIE.2021.3080202.

[6] X. Zhu, B. Zhang and K. Jin, "Hybrid Nonisolated Active Quasi-Switched DC-DC Converter for High Step-up Voltage Conversion Applications," in IEEE Access, vol. 8, pp. 222584-222598, 2020, doi: 10.1109/ACCESS.2020.3043816.

[7] S. -W. Seo, J. -H. Ryu, Y. Kim and H. H. Choi, "Non-Isolated High Step-Up DC/DC Converter With Coupled Inductor and Switched Capacitor," in IEEE Access, vol. 8, pp. 217108-217122, 2020, doi: 10.1109/ACCESS.2020.3041738.

[8] S. Seo, D. Lim and H. H. Choi, "High Step-Up Interleaved Converter Mixed With Magnetic Coupling and Voltage Lift," in IEEE Access, vol. 8, pp. 72768-72780, 2020, doi: 10.1109/ACCESS.2020.2983757.

[9] K. Li, Y. Hu and A. Ioinovici, "Generation of the Large DC Gain Step-Up Nonisolated Converters in Conjunction With Renewable Energy Sources Starting From a Proposed Geometric Structure," in IEEE Transactions on Power Electronics, vol. 32, no. 7, pp. 5323-5340, July 2017, doi: 10.1109/TPEL.2016.2609501.

[10] P. Zolfi, S. Vahid and A. EL-Refaie, "A Novel Three-Port DC-DC Converter for Integration of PV and Storage in Zonal DC Microgrids," 2021 22nd IEEE International Conference on Industrial Technology (ICIT), 2021, pp. 285-291, doi: 10.1109/ICIT46573.2021.9453479.

[11] P. Zolfi, A. Ajami and V. Behjat, "An Isolated Three Port DC-DC Converter for Energy Management in Zonal DC Microgrids", *The 33rd International Power System Conference (PSC2018)*, October 2018.

[12] S. Vahid, P. Zolfi, J. Land and A. EL-Refaie, "An Isolated Step-Down Multi-Port DC-DC Power Converter for Electric Refrigerated Vehicles Auxiliary Power Unit System," 2022 IEEE Applied Power Electronics Conference and Exposition (APEC), 2022, pp. 1133-1140, doi: 10.1109/APEC43599.2022.9773710.

[13] P. Zolfi, A. Ajami, " A Novel Three Port DC-DC Converter for Fuel Cell based Electric Vehicle (FCEV) Application" in Renewable Energies and Distributed Generation, The 6th Iranian Conference on (ICREDG2018), 2018.

[14] P. Zolfi, S. Vahid and A. EL-Refaie, "A Novel Non-Isolated Multi-Port DC-DC Converter for Hybrid Streetcar Application," IECON 2021 – 47th Annual Conference of the IEEE Industrial Electronics Society, 2021, pp. 1-7, doi: 10.1109/IECON48115.2021.9589573.

[15] S. Vahid and A. El-Refaie, "Generalized Systematic Approach Applied to Design a Novel Three-Port Power Converter," 2020 IEEE International Conference on Industrial Technology (ICIT), 2020, pp. 542-548, doi: 10.1109/ICIT45562.2020.9067254.

[16] S. Vahid and A. EL-Refaie, "General Approach to Synthesize Multi-Port Power Converters for Hybrid Energy Systems," IECON 2021 – 47th Annual Conference of the IEEE Industrial Electronics Society, 2021, pp. 1-7, doi: 10.1109/IECON48115.2021.9589531.

[17] H. Ardi, A. Ajami and M. Sabahi, "A Novel High Step-Up DC–DC Converter With Continuous Input Current Integrating Coupled Inductor for Renewable Energy Applications," in IEEE Transactions on Industrial Electronics, vol. 65, no. 2, pp. 1306-1315, Feb. 2018.
[18] C. Y. Chan, S. H. Chincholkar and W. Jiang, "Adaptive Current-Mode Control of a High Step-Up DC–DC Converter," in IEEE Transactions on Power Electronics, vol. 32, no. 9, pp. 7297-7305, Sept. 2017.
[19] M. E. S. Ahmed, M. Orabi and O. M. Abdelrahim, "Two-stage micro- grid inverter with high-voltage gain for photovoltaic applications," in IET Power Electronics, vol. 6, no. 9, pp. 1812-1821, November 2013.
[20] A. Rajaei, R. Khazan, M. Mahmoudian, M. Mardaneh and M. Gitizadeh, "A Dual Inductor High Step-Up DC/DC Converter Based on the Cockcroft–Walton Multiplier," in IEEE Transactions on Power Electronics, vol. 33, no. 11, pp. 9699-9709, Nov. 2018, doi: 10.1109/TPEL.2018.2792004.
[21] S. Anand and B. G. Fernandes, "Optimal voltage level for DC microgrids," IECON 2010 - 36th Annual Conference on IEEE Industrial Electronics Society, 2010, pp. 3034-3039, doi: 10.1109/IECON.2010.5674947.
[22] F. Parache, H. Schneider, C. Turpin, N. Richet, O. Debellemanière, É. Bru, AT. Thieu, C. Bertail, C. Marot, "Impact of Power Converter Current Ripple on the Degradation of PEM Electrolyzer Performances," *Membranes*, 2022, 12(2):109, doi: 10.3390/membranes12020109